Submitted to ADVANCED MATERIALS

DOI: 10.1002/adma.((please add manuscript number))
**Article type: Communication**

# Light-Soaking Free Inverted Polymer Solar Cells with an Efficiency of 10.5% by Compositional and Surface Modifications to a Low-Temperature Processed $TiO_2$ Electron Transport Layer

Yu Yan, Feilong Cai, Liyan Yang, Jinghai Li, Yiwei Zhang, Fei Qin, Chuanxi Xiong, Yinhua Zhou, David G. Lidzey, Tao Wang*

Yu Yan, Feilong Cai, Liyan Yang, Jinghai Li, Prof. Chuanxi Xiong, Prof. Tao Wang*
School of Materials Science and Engineering, and State Key Laboratory of Silicate Materials for Architectures, Wuhan University of Technology, Wuhan, 430070, China
E-mail: twang@whut.edu.cn
Yiwei Zhang, Prof. David G. Lidzey
Department of Physics and Astronomy, University of Sheffield, Sheffield, S3 7RH, UK
Fei Qin, Prof. Yinhua Zhou,
Wuhan National Laboratory for Optoelectronics, and School of Optical and Electronic Information, Huazhong University of Science and Technology, Wuhan, 430074, China

Keywords: polymer solar cells, inverted device, metal oxide, light-soaking

Solar cells, such as dye-sensitized solar cells,[1] polymer solar cells[2] and perovskite solar cells,[3] convert the energy of sunlight directly into electricity and have been regarded as a very promising renewable energy source. Polymer solar cells (PSCs) combine advantages of tunability of optoelectronic properties, low-cost solution processability on mechanically flexible substrates.[4] The past couple of years evidence an encouraging progress of PSCs with their power conversion efficiency (PCE) reaching over 10% in both polymer:fullerene[2,5-11] and polymer:non-fullerene[12] bulk heterojunction systems. The routes to break the 10% efficiency barrier include synthesis of new electron donors,[5,10] development of efficient charge transport materials,[7,9,11] morphology control[2,8] and light manipulation with periodic or aperiodic structures.[6]

Among these various approaches to improve device efficiency and stability, new charge transport materials have been demonstrated to be an effective approach.[13] A series of efficient charge transport layers have been developed to satisfy the demands, including the alkali salts,[14] zwitterionic molecules,[15] ionic liquids,[16] n-type metal oxides such as $TiO_x$,[17-19] ZnO,[20-21] $SnO_x$,[22-24] Al-doped ZnO (AZO),[25-26] Mg-doped ZnO (ZnMgO),[27-28] neutral polymers (e.g. PEIE),[29] and conjugated polyelectrolytes (e.g. PFN).[30] Among them, metal oxides are an important class of electron transport materials for inverted PSCs (i-PSCs), and have attracted significant attention. Metal oxides can be processed from solution and their work function can be tuned by compositional modification and surface treatments, allowing

them to act as either a hole transport layer (HTL) or electron transport layer (ETL). Low temperature processed metal oxide ETLs have also been developed to reduce energy consumption and be compatible with PSC fabrication on plastic substrates.[31-32] However, when n-type metal oxide thin films are employed as the ETLs in PSCs devices, they often exhibit S-shaped J-V curves in the initial illumination with lower PCE and FF. Upon continuous light illumination the device metrics gradually recover and finally reach a saturated state, a process known as the "light-soaking" issue.[33-36] This is commonly observed, especially for $TiO_x$, and is regardless of the preparation methods, e.g. sol-gel, atomic layer deposition or high temperature sintering.[35] One way to overcome the light-soaking problem is to chemically dope the metal oxide with other elements, which can reduce its work function and increase its carrier density and consequently reduce the energy barrier between ETL and the photoactive layer.[35-36]

$TiO_2$ benefits from its high transparency and exceptional optoelectronic properties, and can act as the n-type semiconductor in hybrid solar cells or interfacial layer in bulk heterojunction solar cells. Generally, to achieve high performance i-PSCs, anatase or rutile phase $TiO_2$ films are preferred, however high quality $TiO_2$ films require sintering at over 400 $^oC$. Although the sol-gel method enables the fabrication of $TiO_2$ ETL at low-temperature, there are many trap states in such $TiO_2$ films, which also have low crystallinity and conductivity. This greatly deteriorates the performance of the PSCs as well as generating light-soaking issues.[36] Here we synthesize $TiO_2$ nanoparticles (NPs) using titanium tetrachloride as precursor from a low temperature method to create highly crystalline anatase $TiO_2$ nanoparticles having high electrical conductivity.[37-38] We add a titanium chelate, titanium (diisopropoxide) bis(2,4-pentanedionate) (TIPD) which can be converted to titanium oxide bis(2,4-pentanedionate) (TOPD) after losing the isopropoxide group upon thermal annealing, to reduce the porosity and surface roughness of the $TiO_2$ films.[39] With further treatments of the $TiO_2$:TOPD film by UV light irradiation and rinsing with an amine polar solvent ethanolamine (EA), we can substantially increase the PCE and also eliminate the light-soaking issues in these i-PSCs. With photovoltaic blends made of poly[4,8-bis(5-(2-ethylhexyl)thiophen-2-yl) benzo [1,2-*b*:4,5-*b*′]dithiophene-*co*-3-fluorothieno [3,4-*b*]thiophene-2-carboxylate] (known as PTB7-Th, PBDTTT-EFT or PCE10) combined with [6,6]-phenyl-C71-butyric acid methyl ester ($PC_{71}BM$) as the active layer (shown in Figure 1a),[40] we achieved a PCE of 10.5% in a single junction PSC. Our i-PSCs also demonstrate much better stability compared to the acidic and hygroscopic PEDOT:PSS based conventional PSCs (c-PSC), and retain 95% PCE after 600 h store under ambient conditions at ~60% humidity.

The mechanism for the improved PCE and reduced light-soaking issue is discussed through optoelectronic characterizations of the photoactive layer and the ETL.

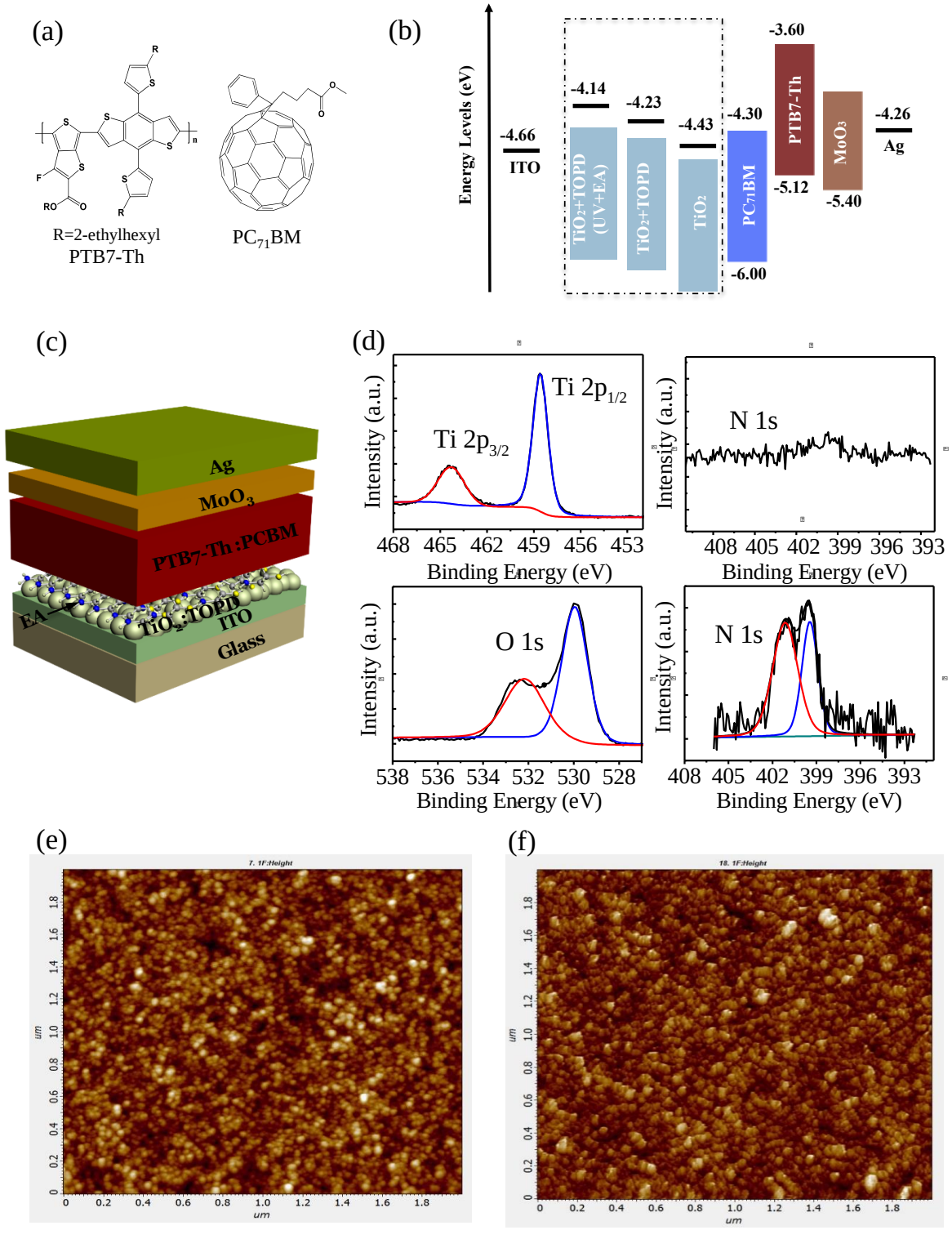


**Figure 1. (a)** Molecular structures of donor polymer PTB7-Th and fullerene acceptor $PC_{71}BM$. (**b**) Energy levels in an inverted device. (**c**) Schematic diagram of an inverted PSC. (**d**) X-ray photoelectron spectroscopy (XPS) of Ti 2p (upper left), O 1s core level spectra (bottom left) of pure $TiO_2$ films and N1s core level spectra of $TiO_2$:TOPD films before (upper right) and after EA treatment (bottom right). Surface morphology of (**e**) TiO2 NPs and (**f**) TiO2:TOPD films cast on ITO substrates.

The device structure of i-PSCs explored is based on glass/ITO/ETL/Active layer/$MoO_3$/Ag. We have also fabricated c-PSCs based on glass/ITO/PEDOT:PSS/Active layer/Ca/Ag. The active layer was cast from a chlorobenzene (CB) solution of PTB7-Th:$PC_{71}BM$ (1:1.5 w/w ratio) containing 3 vol.% of 1,8-diiodooctane (DIO). The device fabrication details are described in experimental section.

The as-synthesized $TiO_2$ NPs were dispersed in 2-methoxyethanol and have found to be stable for several months by storing in a refrigerator (Figure S1a). They have a peak particle size *ca.* 20 nm as determined from our dynamic light scattering measurement using a dispersion with a solid content of 5 mg/ml (Figure S1b), and contain high quality anatase crystals (Figure S1c) with a crystal diameter of approximately 4.5 nm as calculated from the Scherrer equation using the (101) diffraction peak. The ETL films with and without the presence of TOPD were cast from solutions with or without TIPD (shown in Figure S1a) and then thermally annealed at various temperatures, with the conversion of TIPD to TOPD been verified by X-ray photoelectron spectroscopy (XPS) and Fourier Transform Infrared (FTIR) spectra in a previous study.[39] The optimum content of TIPD in $TiO_2$ was determined to be 45% molar ratio, through the comparison of stabilized device efficiency with the addition of different amount of TIPD (see Figure S2a). The optimum temperature was also determined through device studies as shown in Figure S2b. The highest PCE was found when the annealing temperature was at 155 $^oC$, however, 96% of the highest PCE can still be achieved when the annealing temperature is below 100 $^oC$. This slightly lower efficiency most likely results from the incomplete conversion from TIPD to TOPD, although we can not ensure a complete conversion even at the optimum temperature of 155 $^oC$ for a duration of 30 mins performed in this work.

The $TiO_2$:TOPD films were further treated with UV light and EA solvent before the deposition of the photoactive layer. The surface chemical composition of these thin films was evaluated via XPS. Figure 1d shows scans of the Ti 2p, O 1s core level spectra of $TiO_2$ NPs and the N 1s core level spectra of $TiO_2$:TOPD (before and after UV and EA treatments). The Ti $2p_{1/2}$ and Ti $2p_{3/2}$ peaks of a $TiO_2$ NPs film are located at binding energies of *ca.* 458.5 and 464.2 eV, respectively; a finding that indicates that Ti is in a $4^+$ oxidation state in the Ti-O bond. The asymmetric O1s peak detected from the film surface was fitted with two Gaussian components centered at around 529.9 and 532.6 eV. The peak with the lower binding energy corresponds to $O^{2-}$ ions in the anatase structure of $TiO_2$, and the higher binding energy component is associated with the oxygen-deficient regions and the presence of the OH (hydroxyl) bonds. In order to determine the stoichiometry Ti:O from the XPS spectra, the Ti

2p peaks were integrated and elemental sensitivity factors of Ti and O peaks were calculated. The Ti:O ratio in the sample was found to be 2.01, indicating that a small amount of oxygen molecules are absorbed on the $TiO_2$:TOPD film surface during film casting in air. After spin casting of the EA solvent onto the $TiO_2$:TOPD film, typical core line of the N 1s is observed via a weak peak at *ca.* 401.0 eV which can be attributed to the N-O bond formed after EA absorption on the film surface.[38] Furthermore, a Ti-N peak at 399.5 eV is also evident, indicating that the EA molecules on the surface region of the $TiO_2$:TOPD film can dope $TiO_2$.[41]

We now compare the performance of i-PSCs with $TiO_2$-based ETLs having different compositional and surface treatments. The stabilized current density-voltage (J-V) characteristics of the inverted and conventional PSCs under simulated AM 1.5G illumination (100 mW $cm^{-2}$) are plotted in Figure 2a, and the device metrics are summarized in Table 1. The c-PSC reference cell gives a maximum PCE ($PCE_{max}$) of 9.17%. The i-PSC incorporating a pristine $TiO_2$:TOPD film as the ETL gave a $PCE_{max}$ of 9.82% (with $PCE_{ave}$=9.79±0.03%). The main difference between the c-PSC and the i-PSC with a pristine $TiO_2$:TOPD ETL is the improved short-circuit current density ($J_{sc}$) from 16.84 to 18.13 mA $cm^{-2}$, whilst the fill factor (FF) and open-circuit voltage ($V_{oc}$) are similar. This is a significant improvement in device efficiency compared to i-PSC devices containing a pure $TiO_2$ film as the ETL, which have a $PCE_{max}$ of 8.73% (with $PCE_{ave}$=8.35±0.12%) with a large spread in PCE. These results indicate the importance of a dense $TiO_2$:TOPD ETL layer having a smooth interface, as can be characterized by Scanning probe microscope (SPM, Figure 1e and f) and scanning electron microscope (SEM, Figure S3). SPM and SEM images reveal that both $TiO_2$ and $TiO_2$:TOPD ETLs are composed of nanoparticles. However, the $TiO_2$ ETL film contains obvious gaps between particles and SPM measurements indicate a RMS roughness of 7.56 nm. The gaps between particles become smaller and the RMS roughness reduces to 4.32 nm in the $TiO_2$:TOPD ETL. TOPD acts as a binder to enhance the nanoparticle connectivity in the ETL. A dense ETL with a low surface roughness is necessary to ensure intimate contact between the photoactive layer and this reduces the series resistance of device to improve efficiency.

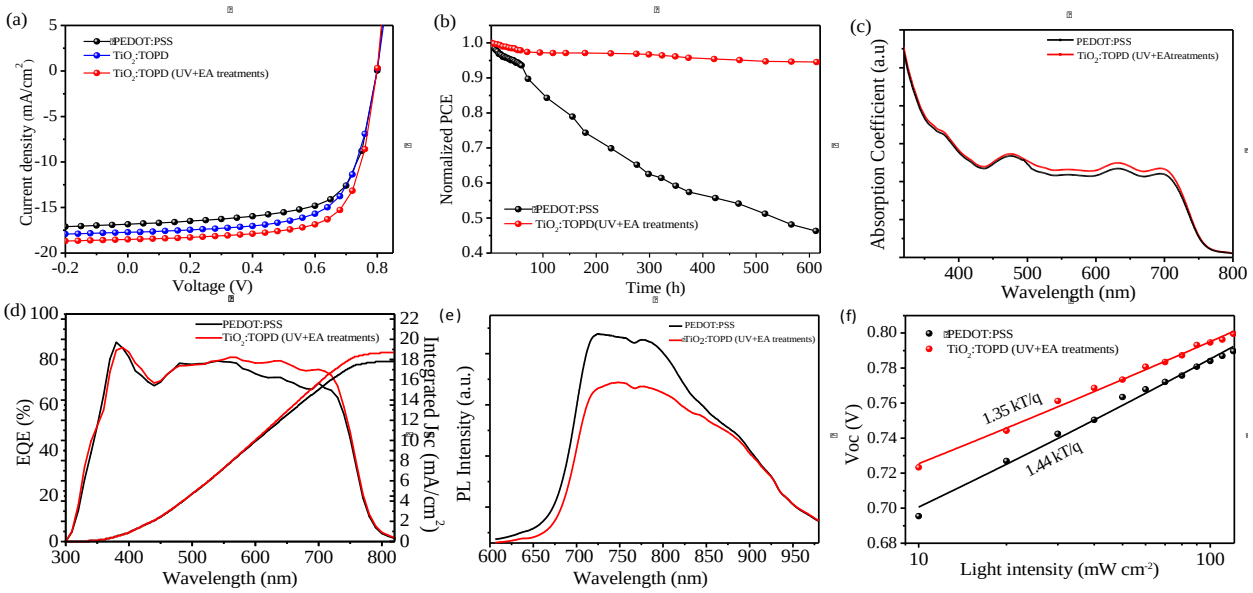


**Figure 2.** (**a**) Stabilized J-V curves of the c-PSC and i-PSCs with $TiO_2$:TOPD and UV+EA treated $TiO_2$:TOPD as ETLs under standard irradiation of 100 mW/cm$^2$. (**b**) Stability, (**c**) absorption, (**d**) external quantum efficiency (EQE), (**e**) photoluminescence and (**f**) light intensity dependent open-circuit voltage of conventional and inverted devices.

The devices with UV and EA treated $TiO_2$:TOPD film as the ETL show the highest $PCE_{max}$ of 10.55% ($PCE_{ave}$=10.23±0.04%), with $J_{sc}$ = 18.84 mA cm$^{-2}$, $V_{oc}$ = 0.79 V, FF = 70.85%. This high PCE can only be achieved in i-PSCs with the UV and EA treated $TiO_2$:TOPD film as ETL. As can be seen from Table 1, i-PSCs with a $TiO_2$:TOPD ETL after either UV light treatment or EA solvent treatment only did not show any improvement. We note that either UV treatment or EA treatment has been demonstrated to be able to improve device efficiency for i-PSCs employing $TiO_2$ or ZnO as the ETL.[42-43] Our results here are not necessarily in contrary to these observations. With the addition of TOPD into the pristine $TiO_2$ NP films, we found that the work function (WF) of the $TiO_2$:TOPD ETL was reduced from -4.43 to -4.23 eV as determined from Kelvin probe measurements (see Figure 1b), which can reduce the energy barrier for charge injection from the photoactive layer to electrode, an effect similar to the beneficial effects of UV or EA treatment. UV treatment only or EA treatment only to the $TiO_2$:TOPD ETL can not further improve the interfacial charge transport as indicated by the negligible WF changes, therefore can not make apparent improvement to device efficiency. Rather, it is the combined effect of UV and EA treatments that improve the PCE over 10%. Compared with the c-PSC device, the i-PSC device with UV and EA treated $TiO_2$:TOPD ETL also demonstrated improved stability. Both c-PSC and i-PSC devices were encapsulated with epoxy glue and glass slices and stored in air with ambient humidity of *ca.*

60%. J-V sweeps were performed everyday and as can be seen from Figure 2b, devices retain 95% of PCE after 600 hours. This compares with the c-PSC device whose efficiency was reduced by more than 50% PCE over the same period.

**Table 1.** Stabilized device metrics of conventional and inverted PSCs with different ETLs. The $PCE_{ave}$±error bar was obtained based on 20 individual devices.

| **Device structure** | **$PCE_{max}$ ($PCE_{ave}$) (%)** | **FF (%)** | **Jsc ($mA/cm^2$)** | **Voc (V)** | **Rs ($\Omega$ $cm^2$)** | **Rsh ($\Omega$ $cm^2$)** |
|---|---|---|---|---|---|---|
| ITO/PEDOT:PSS/Active layer/Ca/Ag | 9.17 (9.12±0.05) | 68.10 | 16.84 | 0.80 | 7.52 | 452.86 |
| ITO/$TiO_2$/Active layer/$MoO_3$/Ag | 8.73 (8.35±0.12) | 62.24 | 18.13 | 0.77 | 6.67 | 576.94 |
| ITO/TOPD/Active layer /$MoO_3$/Ag | 9.24 (9.19±0.08) | 65.03 | 17.78 | 0.80 | 7.84 | 533.67 |
| ITO/$TiO_2$:TOPD/Active layer/$MoO_3$/Ag | 9.82 (9.79±0.03) | 67.80 | 18.09 | 0.80 | 5.74 | 502.31 |
| ITO/$TiO_2$:TOPD(UV and EA treatments)/ Active layer/$MoO_3$/Ag | 10.55 (10.23±0.04) | 70.85 | 18.84 | 0.79 | 5.12 | 542.08 |
| ITO/$TiO_2$:TOPD (UV treatment only)/Active layer/$MoO_3$/Ag | 9.84 (9.74±0.05) | 71.82 | 17.11 | 0.80 | 5.56 | 513.40 |
| ITO/$TiO_2$:TOPD(EA treatment only)/ Active layer/$MoO_3$/Ag | 9.59 (9.48±0.07) | 70.87 | 17.10 | 0.79 | 6.59 | 517.81 |

Optical absorption measurements of photoactive layers cast on $TiO_2$:TOPD and PEDOT:PSS surfaces are shown in Figure 2c. The film on $TiO_2$:TOPD has enhanced absorption over the wavelength range 500 to 750 nm; a result consistent with higher transmittance of the $TiO_2$:TOPD ETL. External quantum efficiency (EQE) measurements also show enhanced light absorption in this range. The integrated current density from the EQE spectra were 18.7 and 17.8 mA $cm^{-2}$ for the i-PSC and c-PSC, respectively. This increased light absorption results in an enhanced $J_{sc}$ of the i-PSC compared with the c-PSC, as can be seen from Figure 2a and Table 1. We have also determined the reflective index (*n*) and extinction coefficient (*k*) of each layer in our c-PSC and i-PSC, and simulated the maximum $J_{sc}$ that each device can generate as a function of film thickness using a transfer matrix (TM) method (Figure S4).[44-45] By comparing the simulated $J_{sc}$ at the first peak, we find that the i-PSC with UV and EA treated $TiO_2$:TOPD ETL generates the highest $J_{sc}$. This is followed by the i-PSC containing a pure $TiO_2$ ETL, with the c-PSC having the lowest $J_{sc}$. Photoluminescence (PL) spectra of the photoactive layer cast on $TiO_2$:TOPD and PEDOT:PSS surfaces are shown in Figure 2e. The PL intensity is more quenched when the

film was cast on a UV and EA treated $TiO_2$:TOPD ETL, suggesting efficient charge transfer from the active layer to the ETL. The light intensity dependent J-V characteristics of c-PSCs and i-PSCs were determined (see Figure S5) and $V_{oc}$ vs light intensity plots are shown in Figure 2f, with the slope of the plot corresponding to the ideality factor of the device. Usually a slope equal to unity suggests bimolecular charge recombination, whilst a slope higher than one suggests trap-assistant charge recombination.[46] We find the slope of i-PSC and c-PSC devices to be 1.35kT/q and 1.44kT/q respectively, indicating that traps contribute to charge losses in both types of devices and are more significant in the c-PSC.

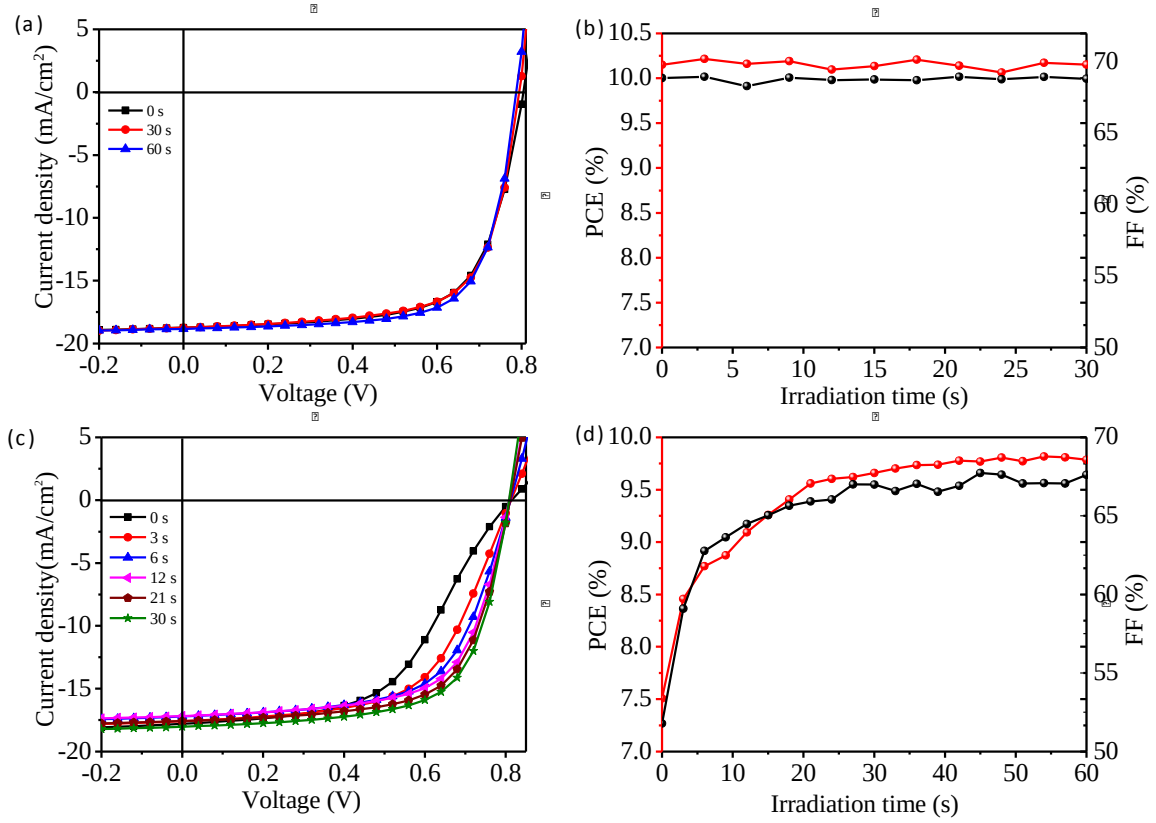


**Figure 3. Light-soaking process of i-PSCs based on $TiO_2$:TOPD ETLs with and without UV and EA treatments.** (**a**) J-V characteristics of inverted PSC device without light-soaking problem after UV and EA treatments, and (**b**) the corresponding evolution in PCE and FF as a function of irradiation time. (**c**) J-V characteristics of inverted PSC device with light-soaking issues without UV+EA treatments, and (**d**) the corresponding evolution in PCE and FF as a function of irradiation time.

The effects of UV and EA treatments on the $TiO_2$:TOPD ETL of i-PSCs not only improve device PCE, but more importantly eliminate the light-soaking issues. In Figure 3a and c we plot J-V characteristics of the i-PSCs with $TiO_2$:TOPD films as ETLs with and without UV and EA treatments, upon various irradiation time under AM 1.5 illumination (100

mW $cm^{-2}$). Figure 3b and d plots the evolution of PCE and FF as a function of time. It can be seen that the i-PSC device with UV and EA treated $TiO_2$:TOPD ETL has reproducible and stable J-V characteristics during the initial J-V sweep and upon different light irradiation times, demonstrating that the absence of a light-soaking problem. However, the i-PSC employing a pristine $TiO_2$:TOPD film without UV and EA treatments show typical light-soaking behavior. The initial J-V sweep is S-shaped, and the J-V curves show increased FF as a function of irradiation time. The PCE and FF of i-PSC based on $TiO_2$:TOPD ETL without any treatments increase gradually and saturate after *ca.* 45 seconds, although it takes a much shorter time to eliminate the light soaking issue compared with some literature report in which over 10 min light irradiation were required until the device stabilized.[34,42,47] The i-PSCs incorporating a pure $TiO_2$ ETL without the presence of TOPD also exhibits light-soaking problem and takes about one minute until the device stabilizes (see Figure S6a and b). The i-PSC device incorporating a pure TOPD ETL exhibits the worst light-soaking issue, and the device stabilizes after a long time *ca.* 6 min (see Figure S6c and d), due to poor charge transport properties at the interface between TOPD and the photoactive layer.

To unravel the effect of UV and EA treatments upon $TiO_2$:TOPD ETL, the optoelectronic characteristics of the $TiO_2$:TOPD ETL and i-PSCs were explored. We first confirmed that the electron mobility of the photoactive layer was unaffected at *ca.* $1.30 \times 10^{-4}$ $cm^2 V^{-1}S^{-1}$, regardless of UV and EA treatments or light soaking (see Figure S7). This electron mobility was extracted from the dark J-V measurements of electron-only glass/ITO/ETL/Active layer/Ca/Ag devices. The conductivity of $TiO_2$:TOPD ETLs with and without UV and EA treatments were also extracted through the J-V characteristics of ITO/$TiO_2$:TOPD/Ag and ITO/$TiO_2$:TOPD(UV and EA treatments)/Ag, and found to have increased from 2.8 to 4.5 x $10^{-3}$ S $cm^{-1}$ after UV and EA treatments. We speculate this results from electron transfer from the EA molecules (donated by the electron-rich $–NH_2$ group) to $TiO_2$ NPs which increases electron density, a result induced by illumination even under normal laboratory light. This photoinduced electron transfer has recently been reported to dramatically increase the electrical conductivity of n-type metal oxides.[48] However as the EA molecules are located at the surface of the ETL film, the increase of the bulk electrical conductivity is not significant. The electrical conductivity of the $TiO_2$:TOPD film after UV and EA treatments remains similar, with the conductivity of films without any treatment increase gradually upon light illumination (see Figure 4a). This is most likely the result of desorption of oxygen molecules upon illumination that were previously absorbed on the

$TiO_2$:TOPD film surface during air processing (see Figure 1d). The desorption of such oxygen molecules reduces the trap density in the $TiO_2$:TOPD film and increases the conductivity.

We find that the WF of the $TiO_2$:TOPD ETL was further reduced from 4.23 to 4.14 eV after UV and EA treatments. Previous work has assigned reduced WF to the formation of dipoles at the surface of ETL.[49] However, it is likely that the increased conductivity of ETL also contributes, as a result of increased electron density which can be induced by removing traps (oxygen desorption),[33] trap-filling by photo-generated electrons,[50] and electron transfer from surface molecules.[48] This reduced WF and enhanced electrical conductivity of $TiO_2$:TOPD upon UV and EA treatments will reduce the energy barrier at the interface of ETL/active layer, and facilitate charge injection from the photoactive layer to the ETL. This is evidenced from electrochemical impedance spectroscopy (EIS) measurements as shown in Figure 4b-d. The impedance spectra are asymmetric semi-arcs for both i-PSCs devices, due to the presence of a chemical resistance ($R_\mu$) that is associated with traps at the active layer/ETL interface. These semi-arcs can only be fitted by incorporating a chemical resistance into the equivalent circuit (shown in Figure 4b), with Rs being a series resistance, $R_1$ and $C_1$ the resistance and capacitance of the bulk photoactive layer, and $R_2$ and Q a modification factor associated with the bulk photoactive layer. For i-PSCs incorporating the UV and EA treated $TiO_2$:TOPD ETL, the semi-arcs remain unchanged, whilst those of the i-PSC employing a pristine $TiO_2$:TOPD ETL get smaller and eventually saturate with increasing light soaking time. Data fitting suggests that $R_s$, $R_1$ and $R_2$ barely change for both type of i-PSCs, indicating that the light soaking problem does not originate from a series resistance at the active layer/ETL interface and the bulk photoactive layer. The i-PSC with UV and EA treated $TiO_2$:TOPD ETL shows constant $R_\mu$ (*ca.* 60 ohm $cm^2$) □□□ chemical capacitance ($C_\mu$), however the i-PSC with a pristine TiO2:TOPD ETL has a much higher initial $R_\mu$ (□□□ $C_\mu$). Notably we find that $R_\mu$ ($C_\mu$) reduces dramatically during the first 20 seconds irradiation, and eventually level off. This reduced $R_\mu$ upon light soaking indicates decreased trap density at the active layer/ETL interface, and consequently reduced carrier recombination. This trend is consistent with device efficiency changes shown in Figure 3d, in which rapid PCE and FF enhancements are evidenced in the initial 20 seconds of measurements. Our optoelectronic results therefore suggest that the bulk photoactive layer remains unaffected, but the interfacial characteristics between the $TiO_2$:TOPD ETL and photoactive layer control light-soaking effects, and determine PCE and i-PSCs device stability.

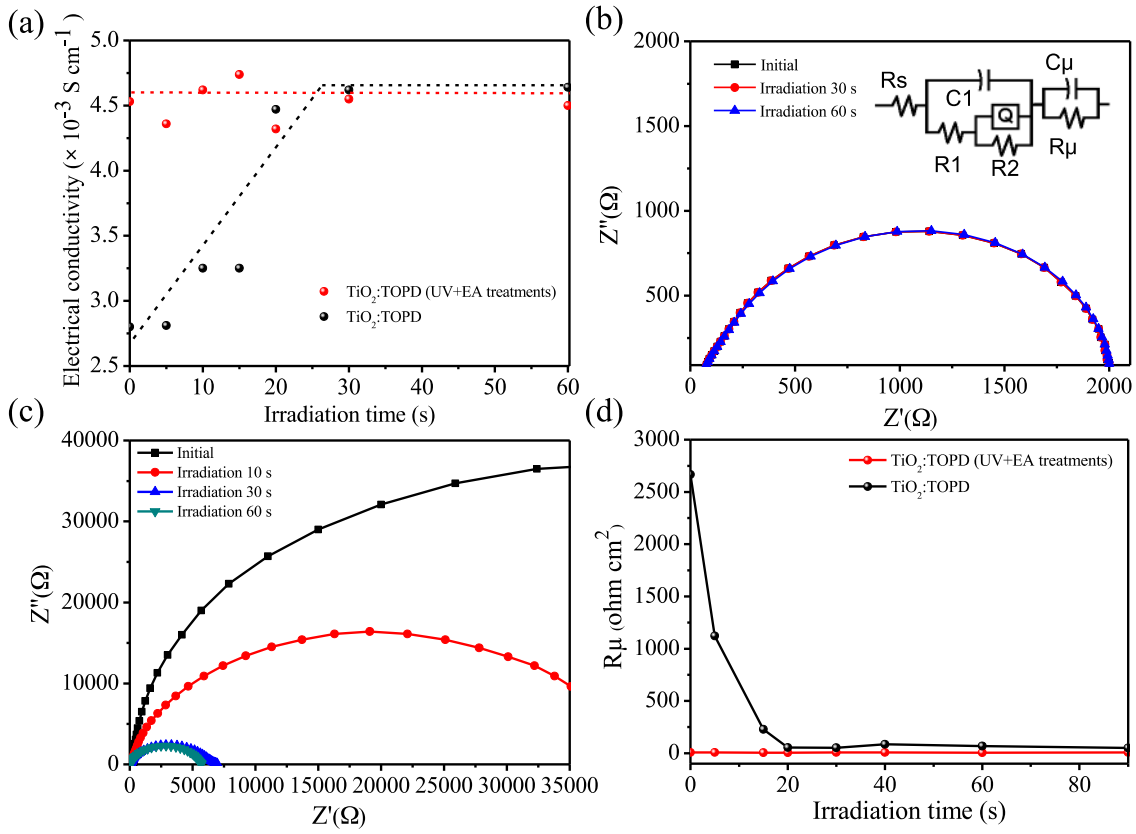


**Figure 4**. (**a**) Electrical conductivity of pristine $TiO_2$:TOPD film and UV and EA treated $TiO_2$:TOPD film. The dashed lines are guide to the eyes. (**b**) and (**c**) are the light-soaking dependent EIS spectra of i-PSCs incorporating the $TiO_2$:TOPD film before and UV and EA treatments. (**d**) Light-soaking dependent interfacial resistance of the i-PSCs.

## Conclusions

In summary, a low-temperature processed $TiO_2$:TOPD electron transport layer was synthesized and treated with UV light irradiation and EA solvent rinsing, and employed as the electron transport layer to fabricate single junction inverted PTB7-Th:$PC_{71}BM$ BHJ solar cells, achieving a best PCE of 10.55% with high fill factor (FF) of 72%. This is one of the best single-junction inverted polymer solar cells reported, and exhibits superior stability under ambient atmosphere compared to conventional device configuration. A low temperature annealing of the $TiO_2$:TOPD ETL below 100 $^oC$ can retain 96% of the highest PCE that was achieved at the optimum annealing temperature of 155 $^oC$. The UV and EA treatments to the $TiO_2$:TOPD ETL not only result in a notable PCE improvement, but also eliminate light soaking issues that are observed in inverted polymer solar cells containing pure $TiO_2$, pure TOPD or pristine $TiO_2$:TOPD as the ETLs. We have therefore demonstrated a promising method to modify metal oxide films without any bulk chemical doping process to enable the fabrication of inverted polymer solar cells with excellent stability and high efficiency.

**Experimental Section**

**Synthesis of $TiO_2$ nanoparticles.** $TiO_2$ nanoparticles were synthesized following a reported anhydrous route.[37] Specifically, 2.3 ml of anhydrous titanium tetrachloride (99.9%) was added dropwise into a beaker containing 8 mL of anhydrous ethanol that was stirred in an ice-water bath. The solution was then transferred into a 100 mL flask containing 40 mL anhydrous benzyl alcohol. The solution was kept at 80 $^oC$ for 9 hours and then precipitated and purified three times with diethyl ether. During each purification process, 27 ml of diethyl ether was added into 3 ml solution before centrifuging at 4000 rpm for 10 min. The precipitate was collected and dispersed in 2-methoxyethanol by ultra-sonication to prepare a $TiO_2$ dispersion with a solid content of ~5 mg/ml. To modify the $TiO_2$ dispersion, 30 ul titanium (diisoproxide) bis(2,4-pentanedioante) (TIPD) was added into 2 ml $TiO_2$ dispersion, and the dispersion was stored in a refrigerator and left to stand for at least 48 h to reach an optimized state before use.

**Device fabrication and testing.** To fabricate OPV devices, pre-patterned ITO-glass substrates (resistance ca. 15 Ω per square) were cleaned by ultrasonication sequentially in water, acetone, ethanol and isopropyl alcohol for 10 min each and then dried at 140 $^oC$ on a hotplate. Cleaned ITO substrates were further treated with UV-$O_3$ for 10 min. The $TiO_2$ electron transport layer was cast from the $TiO_2$/TIPD dispersion at 3000 rpm, followed by thermal annealing at 155 $^oC$ for 30 minutes to create a ca. 20 nm thick thin film. All the processes were performed in an ambient environment. The film was then transferred into an $N_2$-filled glove box and irradiated 5 min under a 254 nm UV light before spin casting the EA solution (1 wt% in 2-methoxyethanol) at 3000 rpm. Finally the $TiO_2$ film was annealed at 125 $^oC$ to remove any residual solvent before putting the photoactive layer on.

The PTB7-Th (14.4 mg/ml) (purchased from Solarmer Materials Inc.) and $PC_{71}BM$ (21.6 mg/ml) solutions were prepared using chlorobenzene (CB) as solvent, and were mixed together with a 1:1.5 w/w ratio to create blend solution having a solid content of 18 mg/ml. 3 vol.% of 1,8-diiodooctane (DIO) was then added to the blend solution and stirred for 3 hours before use. The photoactive layer was cast at 600 rpm onto the $TiO_2$ layer create a film thickness of ~100 nm. The device substrates were transferred into an evaporation chamber and kept overnight under a high vacuum (~$10^{-7}$ torr) to completely remove the residual solvent. Finally, 10 nm $MoO_3$ and 100 nm Ag were deposited onto the photoactive layer through shadow masks by thermal evaporation. For comparison, the conventional PSCs were fabricated using PEDOT:PSS as the hole transport layer. First, 40 nm thick PEDOT:PSS

(Clevios AI 4083, Heraeus, Germany) films were spin-coated onto cleaned ITO substrates, then dried at 135 $^{o}$C for 20 min before depositing the photoactive layer on following the same procedure as described above. Then 5 nm Ca and 100 nm Ag were thermally evaporated forming a cathode under high vacuum. Each device substrate contains 8 pixelated sub-devices, with the size of each active area being 4 mm$^2$ as defined by the shadow mask. All the devices were encapsulated with UV-curable epoxy glue and glass slides before removing from the glove box for device testing.

The absorption spectra of the photoactive layer were extracted by data fitting of the ellipsometry measurements (J. A. Woollam, USA). XPS measurements were performed by using a Thermo Fisher Scientific PHI Quantera II system with a monochromatic Al $K_\alpha$ source. Surface morphologies of the $TiO_2$ films were characterized by SPM (NT-MDT, Russian) and SEM (Hitachi S4800, Japan). Film thickness was measured using a Dektak XT surface profiler (Bruker, USA) and ellipsometry. Work function measurements were performed on a Kelvin probe system (KP020, KP Technology, UK) in air using a highly ordered pyrolytic graphite (HOPG) as the reference sample with a work unction of 4.5 eV.

Device characterization was performed under AM 1.5G(100 mW cm$^{-2}$) using a Newport 3A solar simulator in air at room temperature. The light intensity was calibrated using a standard silicon reference cell certified by the National Renewable Energy Laboratory (NREL). J-V characteristics were recorded using J-V sweep software developed by Ossila Ltd. (Sheffield, UK) and a Keithley 2612B source meter unit. An aperture mask was placed over the devices to accurately define a test area of 2.12 mm$^2$ on each pixel and to eliminate the influence of stray and wave guided light. External quantum efficiency (EQE) was measured with a Newport EQE system equipped with a standard Si diode. The conductivity of the $TiO_2$ films was calculated from the I-V curves of the ITO/$TiO_2$/Ag devices and was defined as $\sigma=h/(RA)$ , with $R$ as electrical resistance ($V/I$), $A$ as the cross-sectional area (4 mm$^2$) and $h$ as film thickness. Impedance measurements were performed on the CHI660E electrochemical workstation (CH instruments, Inc.) under a bias of 0.7 V with the amplitude of 50 mV. The PSCs were soaked under simulated one sun for different time and then measured under dark conditions from high to low frequency (1M to 100 Hz). Equivalent circuit simulations were conducted using the software package ZView 3.1 (Scribner Associate, Inc.).

**Supporting Information**

Supporting information is available from the Wiley Online Library or form the authors.

**Acknowledgements**

The work is supported by the Recruitment Program of Global Experts (1000 Talents Plan) of China, the National Natural Science Foundation of China (Grant No. 21504065, 21474035), and the Fundamental Research Funds for the Central Universities (WUT: 2015III018 and 2015III029) of China. Y.Z. thanks the University of Sheffield for a PhD scholarship.

Received: ((will be filled in by the editorial staff))
Revised: ((will be filled in by the editorial staff))
Published online: ((will be filled in by the editorial staff))

**References**

[1] M. Gratzel, R. A. J. Janssen, D. B. Mitzi, E. H. Sargent, *Nature* 2012, 488, 304.

[2] J. Zhao, Y. Li, G. Yang, K. Jiang, H. Lin, H. Ade , W. Ma, H. Yan , *Nat. Energy* 2016, 2, 15027.

[3] M. Liu, M. B. Johnston , H. J. Snaith , *Nature* 2013, 501, 395

[4] A. J. Heeger, *Adv. Mater.* 2015, 26, 10.

[5] H. Hu, K. Jiang, G. Yang, J. Liu, Z. Li, H. Lin, Y. Liu, J. Zhao, J. Zhang, F. Huang, Y. Qu, W. Ma, H. Yan, *J. Am. Chem. Soc.* 2015, 137, 14149

[6] J. D. Chen, C. H. Cui, Y. -Q Li, L. Zhou, Q.-D. Ou, C. Li, Y. F. Li, J.-X. Tang, *Adv. Mater.* 2015, 27, 1035.

[7] X. Ouyang, R. Peng, L. Ai, X. Zhang, Z. Ge, *Nat. Photonics* 2015, 9, 520

[8] J. Huang, J. H. Carpenter, C. Li, J. Yu, H. Ade, A. K. Y. Jen, *Adv. Mater.* 2015, 5, 1500577.

[9] S. Nam, J. Seo, S. Woo, W. H. Kim, H. Kim, D. D. C. Bradley, Y. Kim, *Nat. Commun.* 2015, 6, 8929

[10] C. Liu, C. Yi, K. Wang, Y. Yang, R. S. Bhatta, M. Tsige, S. Xiao, X. Gong, *ACS Appl. Mater. Inter.* 2015, 7, 4928

[11] W. Yu, L. Huang, D. Yang, P. Fu, L. Zhou, J. Zhang, C. Li, *J. Mater. Chem. A* 2015, 3, 10660

[12] W. Zhao, D. Qian, S. Zhang, S. Li, O. Inganas, F. Gao, J. Hou, *Adv. Mater.* 2016, 28, 4734

[13] Z. Yin, J. Wei, Q. Zheng, *Adv. Sci.* 2016, 1500362

[14] C. S. Kim , S. Lee, L. L. Tinker , S. Bernhard, Y. L. Loo, *Chem. Mater.* 2009, 21, 4583

[15] K. Sun, B. M. Zhao, A. Kumar, K. Y. Zeng, J. Y. Ouyang, *ACS Appl. Mater. Inter.* 2012, 4, 2009 .

[16] W. Yu, L. Huang, D. Yang, P. Fu, L. Zhou, J. Zhang, C. Li, *J. Mater. Chem. A* 2015, 3, 10660.

[17] B. Ecker, H. J. Egelhaaf, R. Steim, J. Parisi, E. Hauff, *J. Phys. Chem. C* 2012, 116, 16333.

[18] S. H. Park, A. Roy, S. Beaupre, S. Cho, N. Coates, J. S. Moon, D. Moses, M. Leclerc, K. Lee, A. J. Heeger, *Nat. Photonics* 2009, 3, 297.

[19] Z. G. Yin, Q. D. Zheng, S.-C. Chen, J. X. Li, D. D. Cai, Y. L. Ma, J. J. Wei, *Nano Research* 2015, 8, 456.

[20] Y. Sun, J. H. Seo, C. J. Takacs, J. Seifter, A. J. Heeger, *Adv. Mater.* 2011, 23, 1679

[21] Z.Q. Liang, Q. F. Zhang, L. Jiang, G. Z. Cao, *Energy Environ. Sci.* 2015, 8, 3442.

[22] S. Trost, A. Behrendt, T. Becker, A. Polywka, P. Görrn, T. Riedl, *Adv. Energy Mater.* 2015, 5, 1500277

[23] B. Bob, T.-B. Song, C.-C. Chen, Z. Xu, Y. Yang, *Chem. Mater.* 2013, 25, 4725

[24] M. Marikkannan, V. Vishnukanthan, A. Vijayshankar, J. Mayandi, J. M. Pearce, *AIP Adv.* 2015, 027122.

[25] T. Stubhan, I. Litzov, N. Li, M. Salinas, M. Steidl, G. Sauer,K. Forberich, G. J. Matt, M. Halik, C. J. Brabec, *J. Mater. Chem. A* 2013, 1, 6004.

[26] X. H. Liu, X. D. Li, Y. R. Li, C. J. Song, L. P. Zhu, W. J. Zhang, H.-Q. Wang, J. F. Fang, *Adv. Mater.* 2016, DOI: 10.1002/adma.201601814.

[27] Z. G. Yin, Q. D. Zheng, S. -C. Chen, D. D. Cai, Y. L. Ma, *Adv. Energy Mater.* 2016, 6, 1501493.

[28] Z. G. Yin, Q. D. Zheng, S. -C. Chen, D. D. Cai, L. Y. Zhou, J. Zhang, *Adv. Energy Mater.* 2014, 4, 1301404.

[29] Y. Zhou, C. Fuentes-Hernandez, J. Shim, J. Meyer, A. J. Giordano, H. Li, P. Winget, T. Papadopoulos, H. Cheun, J. Kim, M. Fenoll, A. Dindar, W. Haske, E. Najafabadi, T. M. Khan, H. Sojoudi, S. Barlow, S. Graham, J. L. Bredas, S. R. Marder, A. Kahn,B. Kippelen, *Science* 2012, 336, 327 .

[30] Z. C. He, C. M. Zhong, S. J. Su, M. X , H. B. Wu, Y. Cao, *Nat. Photonics* 2012, 6, 591.

[31] T. Yang, M. Wang, Y. Cao, F. Huang, L. Huang, J. Peng, X. Gong, S. Z. D. Cheng, Y. Cao, *Adv. Energy Mater.* 2012, 2, 523

[32] F. Xie, W. C. H. Choy, C. Wang, X. Li, S. Zhang, J. Hou, *Adv. Mater.* 2013, 25, 2051

[33] H. Schmidt , K. Zilberberg , S. Schmale , H. Flügge , T. Riedl , W. Kowalsky , *Appl. Phys. Lett.* 2010, *96*, 243305 .

[34] J. Kim , G. Kim , Y. Choi , J. Lee , S. H. Park , K. Lee , *J. Appl. Phys.* 2012, *111*, 114511 .

[35] S. Trost, K. Zilberberg, A. Behrendt, A. Polywka, P. Gorrn, P. Reckers, J. Maibach, T. Mayer, T. Riedl, *Adv. Energy Mater.* 2013, 3, 1437.

[36] G. Kim, J. Kong, J. Kim, H. Kang, H. Back, H. Kim, K. Lee, *Adv. Energy Mater.* 2014, 3,

1401298

[37] K. Wojciechowski, M. Saliba, T. Leijtens, A. Abate, H. J. Snaith, *Energy Environ. Sci.* 2014, 7, 1142

[38] J. Wang, J. J. Polleux, J. Lim, B. Dunn, *J. Phys. Chem. C* 2007, 2, 14925.

[39] Z. A. Tan, W. Q. Zhang, Z. G. Zhang, D. P. Qian, Y. Huang, J. H. Hou, Y. F. Li, *Adv. Mater.* 2012, 24, 1476

[40] S. Zhang, L. Ye, W. Zhao, D. Liu, H. Yao, J. Hou, *Macromolecules* 2014, 47, 4653

[41] J. C. Yu, D. B. Kim, G. Baek, B. R. Lee, E. D. Jung, S. Lee, J. H. Chu, D.-K. Lee, K J. Choi, S. Cho, M. H. Song, *Adv. Mater.* 2015, 27, 3492.

[42] H. Kang, S. Hong, J. Lee, K. Lee, Adv. Mater. 2012, 24, 3005

[43] C. E. Small, S. Chen, J. Subbiah, C. M. Amb, S.-W. Tsang, T.-H. Lai, J. R. Reynolds, F. So, Nat. Photonics 2012, 6, 115.

[44] D. C. Watters, J. Kingsley, H. Yi, T. Wang, A. Iraqi, D. G. Lidzey, *Org. Electron.* 2012, 13, 1401

[45] T. Wang, N. W. Scarratt, H. Yi, I. F. Coleman, Y. W. Zhang, R. T. Grant, J. Z. Yao, M. W. A. Skoda, A. D. F. Dunbar, R. A. L. Jones, A. Iraqi, D. G. Lidzey, *J. Mater. Chem. C* 2015, 3, 4007

[46] C. M. Proctor, M. Kuik, T.-Q. Nguyen, *Prog. Polym. Sci.* 2013, 38, 1941.

[47] M. R. Lilliedal, A. J. Medford, M. V. Madsen, K. Norrman, F. C. Krebs, *Sol. Energy Mater. Sol. Cells 2010*, 94, 2018.

[48] L. Nian, W. Zhang, N. Zhu, L. Liu, Z. Xie, H. Wu, F. Wurthner, Y. Ma, *J. Am. Chem. Soc.* 2015, 137, 6995.

[49] B. R. Lee, E. D. Jung, Y. S. Nam, M. Jung, J. S. Park, S. Lee, H. Choi, S.-J. Ko, N. R. Shin, Y. -K. Kim, S. O. Kim, J. Y. Kim, H.-J. Shin, S. Cho, M. H. Song, *Adv. Mater.* 2014, 26, 494.

[50] C. S. Kim, S. S. Lee, E. D. Gomez, J. B. Kim, Y.-L. Loo, *Appl. Phys. Lett. 2009, 94*, 113302

**The table of contents entry: A promising method is introduced for compositional modification and surface treatments of the $TiO_2$ film prepared from a low temperature route.** Inverted polymer solar cells incorporating the post-treated TiO2:TOPD electron transport layer achieve the highest efficiency of 10.5%, and more importantly, eliminate the light-soaking problem that is commonly observed in metal oxide- based inverted polymer solar cells.

**Keyword:** polymer solar cells, inverted device, metal oxide, light-soaking

Yu Yan, Feilong Cai, Liyan Yang, Jinghai Li, Yiwei Zhang, Fei Qin, Chuanxi Xiong, Yinhua Zhou, David G. Lidzey, Tao Wang*

**Light-Soaking Free Inverted Polymer Solar Cells with an Efficiency of 10.5% by Compositional and Surface Modifications to a Low-Temperature Processed TiO2 Electron Transport Layer**

ToC figure